Analyzing RGB and HSV Color Spaces for Non-Invasive Blood Glucose Level Estimation Using Fingertip Imaging

Asawari Kedar Chinchanikar[1], Manisha P. Dale[2]
Department of Electronics and Telecommunication, AISSMS Institute of Information Technology, Pune, India[1]
Department of Electronics and Telecommunication, MES Wadia College of Engineering, Pune[2]

***Abstract*—Traditional blood glucose measurement methods, including finger-prick tests and intravenous sampling, are invasive and can cause discomfort, leading to reduced adherence and stress. Non-invasive BGL estimation addresses these issues effectively. The proposed study focuses on estimating blood glucose levels (BGL) using "Red-Green-Blue (RGB)" and "Hue-Saturation-Value (HSV) color spaces" by analyzing fingertip videos captured with a smartphone camera. The goal is to enhance BGL prediction accuracy through accessible, portable devices, using a novel fingertip video database from 234 subjects. Videos recorded in the "RGB color space" using a smartphone camera were converted into the "HSV color space". The "R channel" from "RGB" and the "Hue channel" from "HSV" were used to generate photoplethysmography (PPG) waves, and additional features like age, gender, and BMI were included to improve predictive accuracy. To enhance the precision of blood glucose estimation, the Genetic Algorithm (GA) was used to identify the most significant and optimal features from the large set of features. The "XGBoost", "CatBoost", "Random Forest Regression (RFR)", and "Gradient Boosting Regression (GBR)" algorithms were applied for blood glucose level (BGL) prediction. Among them, "XGBoost" yielded the best results, with an R^2 value of 0.89 in the "RGB color space" and 0.84 in the "HSV color space", showcasing its superior predictive ability. The experimental outcomes were assessed using "Clarke error grid analysis" and a "Bland-Altman plot". The Bland-Altman analysis showed that only 7.04% of the BGL values fell outside the limits of agreement (±1.96 SD), demonstrating strong agreement with reference values.**

***Keywords*—Blood glucose; Photoplethysmography; non-invasive; Genetic Algorithm; XGBoost; RGB; HSV**

I. INTRODUCTION

"Diabetes" is a severe, endless illness in which the body is unable to produce enough insulin or cannot effectively use the insulin it produces. As per the report of the "International Diabetes Federation (Diabetes Atlas 2021)" [1], the number of individuals with diabetes in "Southeast Asia" is expected to increase by 68%, reaching 152 million by 2045. In 2021, diabetes was the cause of 747,000 fatalities. Over 50% of adults with diabetes remain undiagnosed. This is because current methods are invasive. Invasive methods include laboratory techniques or using glucometers at home. These methods cause discomfort due to the need for pricking, and they only provide a snapshot of glucose levels at that moment. It is very inconvenient for patients having "type-1 or type-2 diabetes" to collect blood samples multiple times a day as they need to adjust their insulin doses and make necessary changes to their diet or physical activities. The discomfort from frequent finger pricks may discourage some patients from regularly monitoring their glucose levels. Hence patients seek more convenient and non-invasive options for continuous glucose monitoring.

"Non-invasive blood glucose estimation" is painless, comfortable, user friendly, economical, minimizes infection risks, offers continuous monitoring, promotes better adherence, and is appropriate for individuals of all ages. Research is ongoing into various "non-invasive blood glucose estimation" methods, including the use of "saliva" [2], "sweat" [3], "photoacoustic spectroscopy" [4], "Mid-infrared (MIR) spectroscopy" [5], "Near-infrared spectroscopy (NIR)" [6-10]. PPG-based near-infrared spectroscopy is highly admired for its ability to provide non-invasive, real-time monitoring of vital physiological parameters, combining the benefits of PPG's surface-level monitoring and NIR's deeper tissue analysis. In this technique, an optocoupler pair that consists of a "light source and detector" in the wavelength range of 700 nm to 2500nm is directed onto the target. This light interacts with the blood components, undergoing scattering, absorption, and reflection. The amount of light received after interaction changes in direct proportion to the BGL in the blood, according to the Beer-Lambert law [11]. By measuring these intensity changes, the receiver can detect and quantify the presence of glucose molecules within the blood vessels.

A smartphone is a versatile and powerful device that can perform various tasks beyond its primary role of communication. As per Statista's report [12], the smartphone user base in India was expected to exceed one billion in 2023 and is estimated to reach 1.55 billion by 2040. Smart phone technology [13] has been advancing rapidly in the healthcare industry, driven by high-resolution cameras, built-in sensors, innovative applications, and enhanced network connectivity with healthcare providers. Due to technological advancements, smartphone cameras can now function as sensors and can be used to estimate heart rate[14], hemoglobin [15-20], blood glucose [16-17], [21-22], and breast cancer [23].

There is an option to use different color spaces to estimate various physiological parameters from a video recorded with a smartphone. Researchers have reported varying performance levels depending on the selection of color pixels from videos. In [15-17], the "RGB color space" was utilized to estimate hemoglobin and blood glucose levels. Hasan et al. [18]

transformed "RGB" video data into different color spaces, such as "hue (H), saturation (S), value (V), lightness (L), a, b (a and b for the color dimensions) and gray (g)" to estimate hemoglobin. Hasan et al. [19], observed that the "RGB" pixel intensities of video frames were transformed into the "HSV color space" for hemoglobin level estimation. Fan et al. [20], utilized the "a parameter" of the "L*a* b color space" to predict hemoglobin concentration. The Red channel in "RGB color space" is more susceptible to lighting variations, leading to noise in the signal. In contrast, the "Hue channel" in "HSV color space" is more resilient to lighting fluctuations, making it a better choice in uncontrolled or variable lighting conditions.

In previous studies, BGL estimation from fingertip videos has predominantly relied on features extracted from the "RGB color space". However, the "RGB color space" may not always fully capture the range of information relevant to blood glucose levels, as it is sensitive to variations in lighting and may not effectively represent subtle color changes associated with physiological fluctuations. To address this limitation, the proposed study opted to explore both "RGB" and "HSV color spaces" independently. The "HSV color space" offers distinct advantages over "RGB color space", as it separates color information into three components: "hue, saturation, and value". This separation enhances its ability to handle lighting variations and makes it more sensitive to color changes that are linked to physiological changes such as BGL fluctuations. By analyzing and modeling the data separately in both "RGB" and "HSV color spaces", the proposed study aimed to compare the effectiveness of each color space in capturing relevant features for accurate BGL estimation. This dual approach allows for a more comprehensive understanding of how each color space contributes to BGL estimation and provides valuable insights into which may be more effective for non-invasive glucose monitoring. The comparative evaluation of "RGB" and "HSV" can help identify optimal feature extraction methods, ultimately improving the robustness and reliability of predictive models for blood glucose estimation.

Proposed study recorded fingertip videos using a smartphone camera and an external light source. The recorded videos were processed in "RGB" and "HSV color spaces", with the "RGB" pixels being converted into the "Hue, Saturation, and Value (HSV)" representation. PPG signals were extracted from the captured video in both color spaces. Machine learning models were developed to forecast BGL based on features derived from the "PPG signal". The performance of both color spaces was analyzed. The main aspects of proposed work are included:

1) One significant contribution of this work is the creation of a new fingertip video database, which features recordings from 234 subjects.

2) A custom stabilization box was designed and developed to securely hold the Near-Infrared (NIR) LED module, the finger, and the smartphone camera, ensuring stability during fingertip video recording.

3) A Streamlit-based application was developed to assess the quality of recorded fingertip videos for PPG signal extraction. This tool facilitated the efficient evaluation of video recordings, ensuring they met the required quality standards for successful signal extraction.

4) As part of the contribution, "RGB" and "HSV color spaces" were utilized to estimate BGL, with "RGB" pixel values converted into the "HSV color space". The model's performance was evaluated in both color spaces to assess the impact of color representation on model accuracy.

The paper is organized as follows: Section II provides a review of the literature, highlighting key studies and methodologies relevant to the field. Section III offers an overview of the proposed system and methodology. Section IV focuses on the processing of PPG signals in detail, while Section V delves into the details of the feature extraction process. Section VI covers feature selection and model construction, emphasizing the methods employed to create an accurate prediction model. Section VII showcases the study's findings, and finally, Section VIII wraps up the paper, emphasizing the key findings and contributions of the work.

II. Related Work

Recent work has emphasized various "non-invasive techniques" for monitoring BGL. Researchers have utilized sensors to estimate BGL by analyzing interstitial fluid. Specific sensors were designed to measure BGL based on optical and non-optical techniques.

Rodin et al. [3], developed a biosensor for measuring blood glucose through sweat analysis. The results were stored on a smartphone linked via "Bluetooth". They calculated the "Mean Absolute Percentage Error (MAPE)" by comparing the obtained values with those from a glucometer using a t-test. Accuracy was assessed through correlation analysis, and "linear regression (LR)" was applied, revealing a maximum error range of 7.40 to 7.54%. The study involved 200 subjects.

Wei et al. [24] assessed BGL using the Skin Oxygen Saturation Imaging System (SOSI) to estimate glucose levels based on light absorption differences. The setup included a Flea 2 CCD camera, an infrared thermal camera, and calibration tools for accuracy. Five subjects aged 22 to 46 participated, with glucose levels monitored before and after meals. Oxygen saturation data was analyzed to estimate glucose concentrations, showing a postprandial glucose increase with variations from 0.38 to 0.92 mmol/L. However, the limited sample size of only five subjects is a drawback, requiring further studies with larger populations to validate the findings and improve reliability.

PPG acquired by pulse oximeter, which works in the NIR region, is an affordable, "non-invasive optical technique" that detects variations in the blood flow within arteries. Monte- Moreno [6], employed a PPG sensor to record the PPG signal and an "activity detection module" to filter out artifacts and avoid signal loss due to finger movement. Additionally, a "signal processing module" was used to derive the primary features. PPG data was recorded for 410 individuals. The predictive models included "Ridge linear regression", a "Multilayer perceptron neural network", "Support Vector Regression (SVR)", and "RFR". Out of these models, the "RFR" delivered the best result with an "R2 value" of 0.90.

Habbu et al. [7], proposed a data acquisition system based on optical sensors operating at 920 nm to record PPG signals. The PPG data was collected for 611 subjects, with each session lasting 3 minutes. They extracted 28 features through single pulse analysis and trained a neural network, achieving an R2 value of 0.91.

Jain et al. [8], developed a system utilizing "NIR spectroscopy" and "machine learning". The device is integrated within an "Internet of Medical Things (IoMT) framework", allowing patients and doctors to access it via the cloud. A noninvasive glucometer has been introduced, utilizing "short NIR waves" with "absorption" and "reflectance of light" at "specific wavelengths, 940 nm and 1,300 nm". A "Deep Neural Network model (DNN)" was employed, and the accuracy was evaluated using Clarke Error Grid analysis, achieving 100% accuracy. The study involved 97 participants.

Joshi et al. [9], proposed using NIR spectroscopy within an IoMT framework for glucose monitoring. A "dual NIR spectroscopy" technique has been proposed, incorporating "absorption and reflection spectroscopy" at 940 nm and absorption spectroscopy at 1,300 nm. "DNN" was implemented for sensor calibration, while "polynomial regression models" were utilized to predict serum glucose levels. 200 subjects were included and reported an accuracy of 100%.

Recently, many smartphones have incorporated sensor systems that enable real-time heart rate and oxygen saturation measurement through PPG. These non-invasive techniques are becoming increasingly popular due to their distinct benefits, such as ease of use, painlessness, no risk of infection, and the ability to deliver instant results. Golap et al. [16], proposed imaging plethysmography (IPPG) for estimating blood glucose and hemoglobin levels. Fingertip videos were recorded with a smartphone camera, using a NIR LED board for light illumination. The NIR board comprised 850 nm NIR LEDs and one flash LED. A 15-second video was captured from 111 subjects. "RED channel" was employed to extract the "PPG signal". A 500 × 500-pixel section was selected from the right- to-left part of the frame as a "Region of Interest (ROI)". Forty-six "time and frequency domain" features, along with age and gender, totalling 48 features, were used to train the predictive model. Correlation-based feature selection through "Multigene Genetic Programming" (MGGP) was recommended. "SVR", "LR", "RFR", and "MGGP symbolic regression" were employed. The MGGP-based model achieved an R2 value of 0.88 on the test dataset.

Haque et al. [17], developed a "DNN" model to access hemoglobin, glucose, and creatinine levels using "PPG signals". A NIR LED board (850 nm) and a "smartphone camera" was used to record fingertip videos, and the "PPG signal" was extracted from the "RED channel". A 500 × 500-pixel section from the right-to-left portion of the image was chosen as the ROI. The study included 93 subjects, and 48 "time and frequency domain features", including age and gender, were derived. "Correlation-based feature selection (CFS)" with "Genetic Algorithms (GA)" was employed and achieved an R2 value of 0.902 for estimating BGL.

Islam et al. [22] used a front-facing camera to capture fingertip videos from 52 subjects, recording between 20 to 50 seconds. The "RED channel" was selected to derive the "PPG signal". Various predictive models to estimate glucose levels, including "Principal Component Regression (PCR)","Partial Least Squares Regression (PLS)", "SVR", and "RFR". Among these models, the "PLS model showed the optimum "standard error of prediction (SEP)" at 17.02 mg/dL.

Limited research has been conducted on non-contact BGL estimation. Nie et al. [25], developed the technique for BGL prediction based on IPPG combined with machine learning. The near-infrared industrial camera operating at 940 nm was used to capture video from the face, focusing on the cheek area as the region of interest. The study involved eight adults who recorded 1-minute videos. A total of 1280 videos were collected along with an oral glucose tolerance test (OGTT). Weighted averaging of pixel values were used to extract the PPG signal, from which 26 features were derived, including time-domain, energy- domain, and human physiological parameters. Correlation-based feature selection was employed and tested various machine-learning models, including "PCR, SVR, RFR, and PLS". The best results were achieved with RFR, reporting a "Mean Absolute Error (MAE)" of 1.72 mmol.

Different approaches have been investigated to process "PPG signals", extract prominent features, and optimize these features for improved performance. Chen et al. [26], presented a novel algorithm to detect "beat onsets and peaks" from noisy "PPG waveforms". Subohet al. [27], explored the use of derivative waveforms and inflection points for accurate detection of PPG, VPG, and APG peaks, enhancing diagnostic precision. McDuff et al. [28], introduced an automated approach for identifying "systolic and diastolic peaks" in a "PPG waveform" recorded remotely with a digital camera. Takazawa et al. [29], highlighted that the "second derivative of the PPG (SDPTG) waveform" serves as a valuable indicator of vascular health. Specifically, the b-c-d-e/a ratio has been widely used to assess vascular aging and the influence of vasoactive agents, making it particularly relevant in the evaluation of cardiovascular conditions. Rubins et al. [30] demonstrated that PPG-derived parameters, including "Digital Volume Pulse (DVP), augmentation index (AIx), and reflection index (RI)", exhibit significant variations between healthy individuals and cardiovascular patients. Esper et al. [31], highlighted that arterial waveform analysis, beyond blood pressure monitoring, provides key hemodynamic parameters like "stroke volume (SV), cardiac output (CO), vascular resistance, SV variation (SVV), and pulse pressure variation (PPV)" in clinical settings. Seitsonen et al. [32], highlighted the importance of multimodal monitoring in assessing analgesic adequacy, demonstrating that a logistic regression model incorporating "EEG response entropy, ECG RR-interval, and PPG notch amplitude" achieved the highest classification accuracy. Baek et al. [33], introduced the "second derivative of photoplethysmography (SDPTG)" as an advanced application of PPG for assessing arterial stiffness and aging. The SDPTG waveform comprises five distinct waves as a, b, c, and d in the "systolic phase" and e in the "diastolic phase" with its pattern defined by the ratios of the b, c, d, and e waves to the primary a wave. Xiao et al. [34], demonstrated that the "Stress- Induced Vascular Response Index (sVRI)", derived from "PPG", effectively assesses cognitive load during gaming, enabling real-time evaluation of players" mental workload and

informing game design optimizations. “Genetic Programming” (GP), introduced by Koza [35], is an evolutionary algorithm that evolves computer programs to solve problems like Boolean function learning and symbolic regression using principles of “survival of the fittest” and “genetic crossover”. Thanathamathee et al. [36], employed an enhanced XGBoost framework integrating SHAP-based instance weighting and Anchor Explainable AI to address class imbalance and improve interpretability in financial fraud detection.

In existing literature, various sensor-based methods have been employed to estimate blood BGL, demonstrating the potential of non-invasive monitoring. These sensors often require physical contact or attachment to the body, which can limit user comfort and accessibility. In contrast, smartphone cameras have emerged as a promising alternative for BGL estimation, with several studies leveraging the RGB color space to analyze fingertip videos. This approach benefits from the widespread availability of smartphones, offering a practical and affordable option for continuous monitoring.

Previous smartphone-based methods to estimate BGL were limited by small sample sizes, which hindered the ability to draw broad conclusions and generalize findings across diverse populations. Smaller sample sizes failed to adequately represent variations in key demographic factors, such as age, gender, and different glycemic conditions, thereby reducing the robustness and applicability of the results. Furthermore, many studies did not include individuals with varying medical conditions like hypertension or diverse glycemic conditions (e.g., hyperglycemia and hypoglycemia), which were crucial for understanding how these factors could influence blood glucose estimation. In contrast, the proposed study addressed these gaps by using a comparatively larger sample size, which enhanced the robustness and reliability of the findings. The variability in the sample, encompassing a broader range of age groups, gender distributions, and glycemic conditions, ensured a more comprehensive understanding of blood glucose estimation across different population subgroups. This diversity allowed for improved generalization of the results, making the study more applicable to real-world settings where individual health conditions and demographic factors varied widely. By including subjects with conditions such as hypertension and varying glycemic states, the proposed study provided a more accurate representation of the broader population, helping to overcome the limitations of prior research.

Previous research on fingertip video capture using smartphones and NIR-LED boards showed that slight finger movements or camera shakes during data collection could introduce motion artifacts, distorting PPG signals and compromising the accuracy of BGL estimations. Despite efforts to instruct participants to keep their fingers still, these studies overlooked natural movements like finger shifts, hand tremors, and slight camera shifts caused by breathing, all of which could notably affect the quality of the PPG signals. Even subtle variations in video frames could lead to erroneous feature extraction and unreliable blood component level predictions. To address these limitations, the proposed work introduced a custom stabilization box designed to minimize motion artifacts and ensure more stable and consistent video capture. This new approach aimed to improve the reliability of the PPG signal acquisition process by mitigating the effects of unintentional movements during data collection, providing a more robust and accurate estimation of blood components.

Building upon this work, the proposed study explored the effectiveness of the “HSV color space” in estimating BGL alongside the widely used “RGB color space”. Specifically, fingertip videos captured via a smartphone camera were analyzed to evaluate the effectiveness of both color spaces. While the HSV color space is often considered more robust for color-based applications due to its separation of chromatic content. In the reviewed literature, one notable limitation when recording video using a smartphone for BGL estimation was the lack of a built-in mechanism to assess video quality. Even slight movements, whether of the smartphone or the subject, could lead to video distortions or blurriness, significantly affecting the reliability of the data. This resulted in the collection of suboptimal or unusable video data, potentially rendering the entire database ineffective for accurate analysis. To address this issue, a Streamlit-based application was developed in the proposed work. This application enabled immediate quality checks, ensuring that only top-quality, reliable video data was included in the database, thus improving the accuracy and effectiveness of the BGL estimation process.

III. METHODOLOGY

The proposed system model, as illustrated in the Fig. 1, depicts the overall operational flow and operational flow of the setup. It begins with data collection, where relevant information was gathered using smartphone camera. The collected data was then passed through signal extraction and processing steps to remove noise and ensure the data was in a usable format. Following this, feature selection was performed to identify and extract the most significant features that contributed to accurate predictions or classifications. The selected features were subsequently used for model building, where machine learning techniques were applied to develop a predictive or analytical model. This comprehensive flow ensured that the system effectively processed raw data, optimized the input features, and generated accurate, actionable outcomes.

A. Experimental Setup

The hardware setup for the BGL estimating system included a NIR LED module and a smartphone camera. The NIR LED module comprised six surrounding NIR LEDs and one flash LED. The flash LED was employed to enhance the light intensity of the NIR LEDs. The proposed study utilized a 940 nm NIR LED board because blood glucose demonstrates significant absorption properties in the NIR range, with an absorption peak between 940 nm and 1000 nm, as illustrated in Fig. 2.

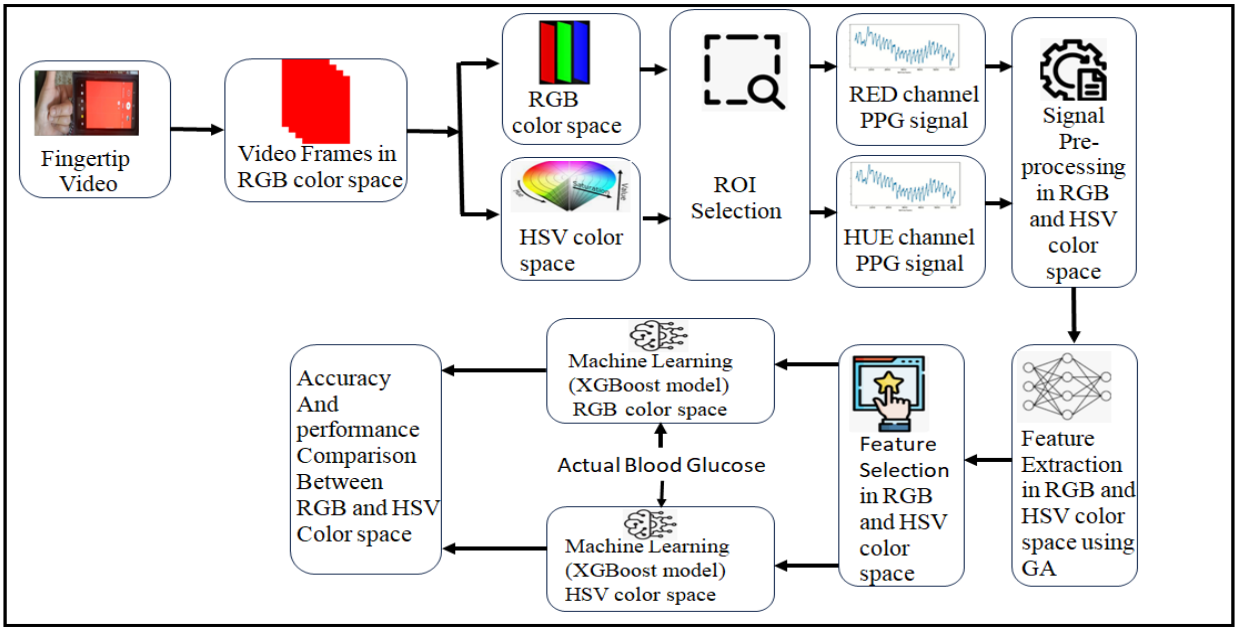

Fig. 1. Proposed model design.

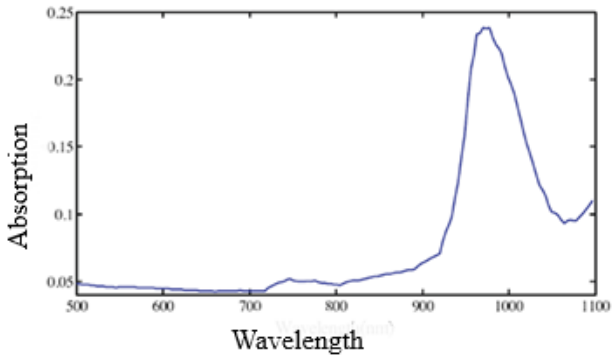

Fig. 2. Absorption spectrum of blood glucose in the NIR light range.

Fig. 3(a) illustrates the NIR LED module, which includes six outer NIR LEDs and a central flash LED, and Fig. 3(b) shows its design. NIR LEDs were employed to illuminate the finger.

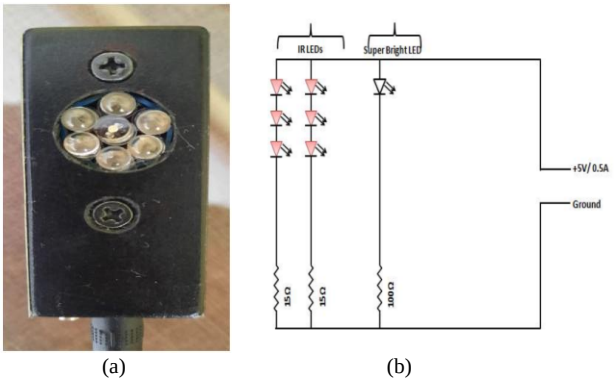

(a) (b)

Fig. 3. (a) NIR LED module, (b) Module design.

B. Data Collection

In proposed study, fingertip videos in *.mp4 format were recorded from 234 subjects, consisting of 122 females and 112 males. The subject's ages ranged from 22 to 88 years, with their weights ranging from 45 to 120 kg. The dataset includes "diabetic" subjects ("Type 1 and Type 2") and "non-diabetic" subjects, with BGL ranging from 90 to 480 mg/dL (milligrams per decilitre). The subjects included in the proposed work were diverse in terms of socio-economic background, physiological condition, dietary habits, workout routines, and weight variations, ensuring a thorough representation of the population. This diversity strengthens the generalizability and robustness of the results. Data collection occurred at various local societal institutions in Pune. A "15-second video" of the "right-hand index fingertip" was recorded for each subject.

The subjects willing to participate in this research were provided with a brief overview of the problem statement. Following this, a consent form was signed by each subject. Additionally, a detailed record of each subject's history was maintained, including information on daily dietary habits, workout routines, and any surgical background. All personal information and identities of the subjects were kept confidential to ensure anonymity and protect their privacy.

The subjects were first instructed to clean their hands with soap and dry them thoroughly. They were then asked to settle down for 5 minutes to ensure a relaxed state before the video recording. Prior to recording the fingertip videos, the subjects applied hand sanitizer to maintain proper hygiene. They were also advised to avoid wearing nail polish to ensure accurate video capture of the fingertip. Once the video recording was completed, BGL was measured using an Accu-Check blood glucometer, which features an enzyme system based on Flavin-dependent glucose dehydrogenase (FAD-GDH) and operates through electrochemical sensing for precise glucose measurement. The subjects were directed to position the tip of their "right index finger" on the "NIR LED module", while the smartphone camera was positioned on the opposite side to record the video. The videos were recorded using a Samsung A51 smartphone, which operates on Android 10 and is equipped

with a 48 MP camera, capturing 30 frames per second at a display size of 1080 x 2400 display dimensions.

Several issues were encountered during data collection with the experimental setup.

- The NIR LED board could shift when the finger was placed on it.
- The finger might also move on the NIR LED board due to discomfort.
- Slight movement of the smartphone camera occurred during video capture, often caused by breathing.

To address these issues, several remedial actions were implemented. The NIR LED board was securely fixed inside an empty box to prevent shifting. A slot was created in the box wall, allowing the finger to be easily placed on the NIR LED board while minimizing movement. Furthermore, a slot was added at the upper section of the box to properly position the smartphone properly, ensuring the camera could record videos without movement. The designed box is demonstrated in Fig. 4.

Despite designing a box to minimize movement while recording the video, extracting a clean PPG signal remained challenging due to interruptions such as sneezing, coughing, or small finger movements caused by breathing. To address this, a Streamlit application was developed. "Streamlit" is an "open-source Python library" that enables the creation of "interactive web applications" for "data science and machine learning projects", allowing users to create web-based interfaces for Python scripts without needing front-end development expertise. The video quality for the extracted PPG signal was evaluated using this Streamlit application. After recording the video with acceptable quality, the blood glucose level was measured using an Accu-Check® instant blood glucose meter. The window of the Streamlit application is displayed in Fig. 5.

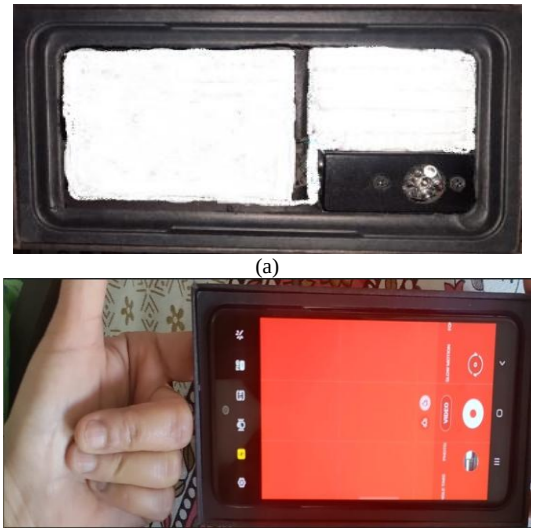

(a) (b)

Fig. 4. (a) Designed box, (b) The finger and smartphone positioned in the designated slots.

Fig. 5. Streamlit application window.

IV. PPG Signal Generation

PPG wave is extracted from recorded fingertip video. The initial "3 seconds" and the final "2 seconds" of the video were removed to remove distorted frames. As a result, 300 frames were extracted from the video for each subject. The recorded videos ware in the "RGB color space". The "PPG signal" was derived from the original videos in the "RGB color space" and the converted "HSV color space" by transforming the "RGB" pixels into "HSV". The conversion of "RGB" to "HSV" consists of normalizing the BGR values to the range [0, 1]; each color component is divided by 255, producing the normalized values B', G', and R'. To determine the maximum (C_{max}) and minimum (C_{min}) values, find the highest and lowest values among the normalized blue, green, and red components. Next, calculate the variation (Δ) between the highest and lowest values. Afterward, the hue (H) is determined by using the following Eq. (1) and (2).

$$H = 60 \times \frac{G' - B'}{\Delta} \quad (\text{if } G' > B') \tag{1}$$

$$H = 60 \times \frac{G' - B'}{\Delta} + 360 \ (\text{if } G' < B') \tag{2}$$

The process for extracting the PPG signal was identical in both color spaces. Choosing the appropriate channel was crucial for extracting the "PPG signal" from a recorded video. The average pixel brightness values for the "Red, Green, and Blue channels" were calculated in the "RGB color space". It was found that the "Red channel" had the greatest pixel intensity, exceeding 200, while the "Green" and "Blue channels" had pixel

values ranging from 60 to 70. Consequently, it was observed that when the pixel intensity in an image was below 200, extracting the key features from the "PPG signal" became challenging. As a result, the "Red channel" was chosen for PPG signal extraction. In the "HSV color space", the Hue channel was used to extract the PPG signal because it directly represents the color type (e.g. red, blue, green) based on its position on the color wheel. Unlike Saturation and Value, which can vary with lighting conditions, Hue is less affected by changes in lighting or brightness. This stability made the "Hue channel" more reliable for PPG signal extraction.

To define the ROI, "K-means clustering" was applied to video frames to segment pixel intensity values into distinct clusters, enabling the identification of the ROI. "K-means clustering" is an "unsupervised machine learning algorithm". The algorithm begins by randomly selecting "K centroids" and then allocates each pixel to the closest centroid in successive steps, recalculating the centroids as the average of the pixel values within each cluster. This process proceeds until the centroids remain unchanged, indicating convergence. In "K-means clustering," inertia was calculated as the total of "squared distances" between each data point and its corresponding "cluster centroid", which indicates how closely the points are grouped within each cluster. The Eq. (3) for inertia is provided, and the elbow graph used to determine the value of K is shown in Fig. 6(a). Fig. 6(b) displays four clusters with distinct pixel intensity values.

$$\text{Inertia} = \sum_{i=1}^{k} (\text{Nearest Centroid distance})^2 \qquad (3)$$

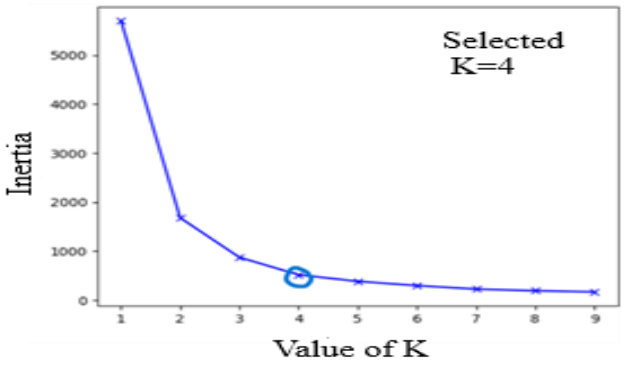

(a)

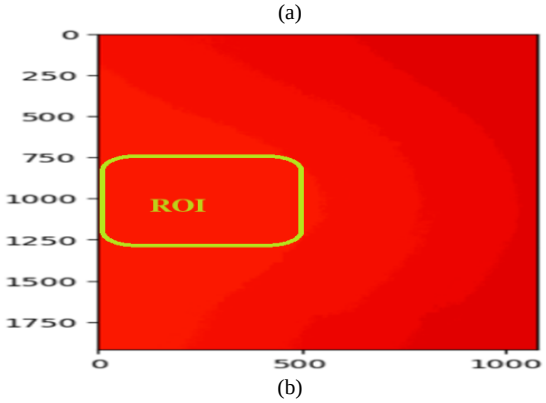

(b)

Fig. 6. (a) Elbow graph, (b) Image frame showing ROI.

Based on the above, a 500x500 pixel region from rows 750 to 1250 and columns 0 to 500 was used as ROI to calculate the average intensity for Red and Hue channels. Thus, the raw PPG signal was obtained by taking mean of the pixel values Eq. (4) of the "red channel" and "Hue channel" within the ROI.

$$PPG(t) = \frac{1}{M \times N} \sum_{i=1}^{M} \sum_{j=1}^{N} PPG(i,j,t) \qquad (4)$$

where, M and N represent the dimensions of the ROI, and PPG(i,j,t) denotes the pixel value at position (i, j) at time t.

Applying suitable preprocessing methods was essential for the precise analysis of the PPG signal. A 10-second video from each subject, consisting of 300 frames, was used. The Butterworth band-pass filter is ideal for pre-processing PPG signals because of its flat passband, sharp roll-off, and consistent performance. Therefore, a "Butterworth BPF filter" with a "low cutoff frequency" of 0.5 Hz and a "high cutoff frequency" of 4 Hz was used to clean the extracted PPG signal in both color spaces, designed to support a heart rate range of 30 to 240 beats per minute. The filtered "PPG signal" is demonstrated in Fig. 7(a).

After filtering the raw "PPG signal", a "peak detection algorithm" was employed to locate the peaks in the signal. Before applying the "peak detection algorithm" to the filtered signal, a moving average filter was applied to reduce noisy fluctuations.

$$y[i] = \frac{1}{K} \sum_{j=1}^{K-1} X[i+j] \qquad (5)$$

Eq. (5) represents a smoothening operation over a sequence X, producing a new sequence y where each element is the average K−1 value from X, starting from index i+1. As a result, the "peak detection algorithm" generated an array of positive and negative peak values. Fig. 7(b) shows the sample plot of the filtered signal in both color spaces after applying the "peak detection algorithm". A "single PPG wave" with the most prominent "positive systolic peak" was selected from the continuous "PPG waveform" extracted from the "Red" and "Hue channels", as illustrated in Fig. 7(c). The flowchart for extracting a "single PPG wave" is shown in Fig. 8. Thus, a clean "PPG signal" was obtained from the video of the index finger in both "RGB" and "HSV color spaces".

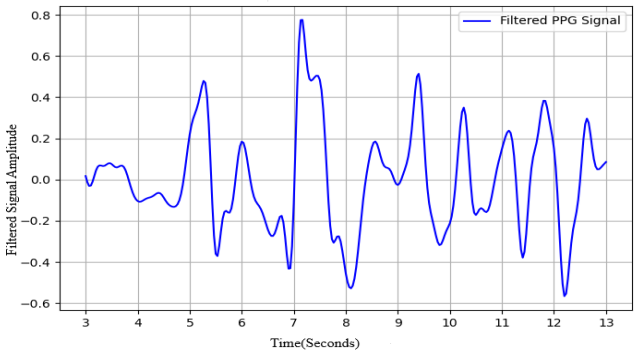

(a)

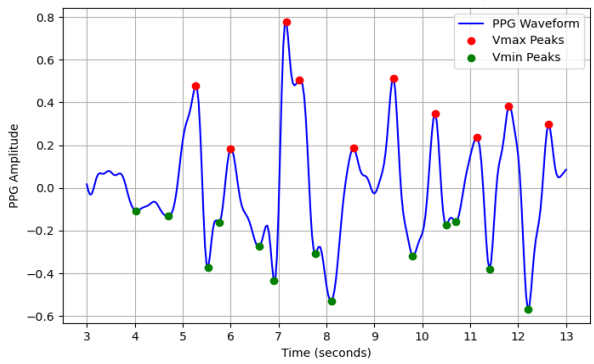

(b)

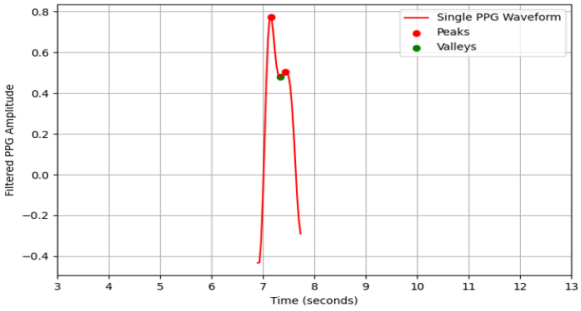

(c)

Fig. 7. (a) Filtered PPG signal, (b) Application of peak detection algorithm to PPG wave, (c) Extracted single PPG waveform with highest peak.

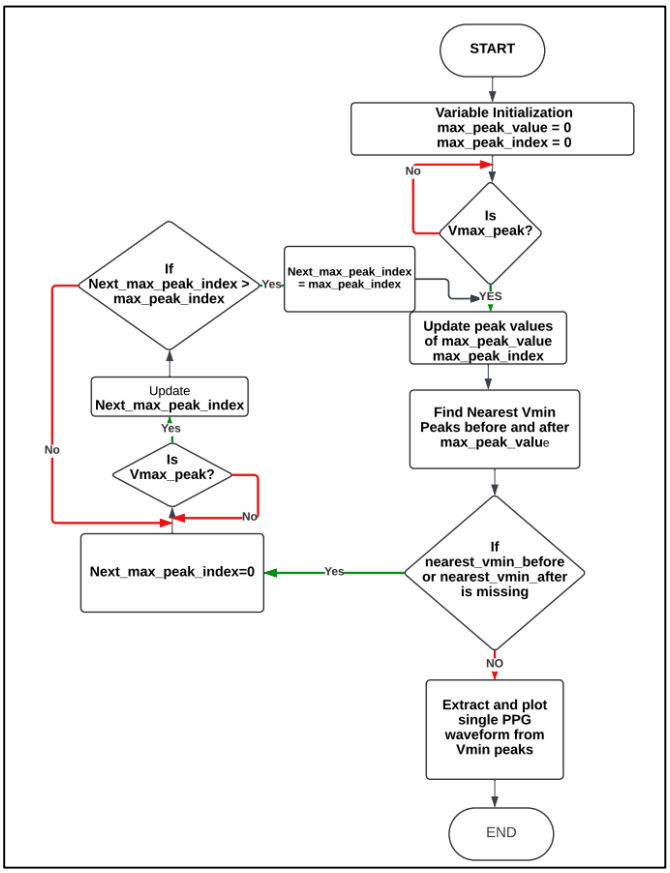

Fig. 8. Flowchart to extract single PPG waveform.

V. Feature Extraction

Once the PPG waveform with the highest peak was extracted from both color spaces, feature extraction is a critical step, as it has a major impact on the performance and accuracy of predictive models. Fig. 9 illustrates the procedure for collecting 49 distinct features, which were obtained from the subject's information and from the "PPG signal's time and frequency domain" analysis. A total of 21 features (f3 to f22 and f48) were derived from the "PPG signal", 19 features were derived from the "first derivative and second derivative" of the "PPG signal" (f23 to f41), and six features (f42 to f47) were obtained by applying the "Fast Fourier Transform (FFT)" to the PPG waveform for each subject in both the color spaces. The extraction of features from the "PPG wave" and its "derivative" is illustrated in the figure. Additionally, the age (f1), gender (f2), and body mass index (f49) of each subject were incorporated in the feature set. The distinct features obtained from the "PPG signal" and its corresponding "first and second derivatives" are shown in Fig. 10. The extracted features are listed in Table I. The process of extracting features in "RGB" and "HSV color spaces" was identical.

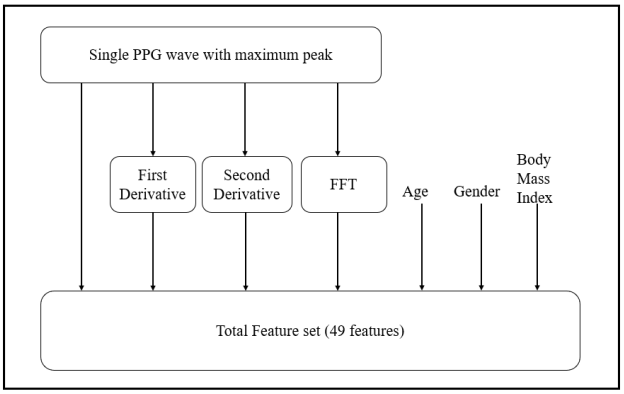

Fig. 9. Schematic diagram of the feature extraction process.

TABLE I. List of Features

Feature	Description	Feature	Description
f1	Age	f26	t_{f1}
f2	Gender	f27	b_2/a_2
f3	x	f28	e_2/a_2
f4	y	f29	$(b_2+e_2)/a_2$
f5	z	f30	t_{a2}
f6	TIP	f31	t_{b2}
f7	y/x	f32	t_{a1}/t_{pi}
f8	(x-y)/x	f33	t_{b1}/t_{pi}
f9	z/x	f34	t_{e1}/t_{pi}
f10	(y-x)/x	f35	t_{f1}/t_{pi}
f11	t_1	f36	t_{a2}/t_{pi}
f12	t_2	f37	t_{b2}/t_{pi}
f13	t_3	f38	$(t_{a1}+t_{a2})/t_{pi}$
f14	Δt	f39	$(t_{b1}+t_{b2})/t_{pi}$
f15	$t_1/2$	f40	$(t_{e1}+t_2)/t_{pi}$

f16	A_2/A_1	f41	$(T_{f1}+t_3)/t_{pi}$
f17	t_1/x	f42	$X(f_0)$
f18	$y/(t_{pi}-t_3)$	f43	$\|X(f_0)\|$
f19	t_1/t_{pi}	f44	$X(f_1)$
f20	t_2/t_{pi}	f45	$\|X(f_1)\|$
f21	t_3/t_{pi}	f46	$X(f_2)$
f22	$\Delta t/t_{pi}$	f47	$\|X(f_2)\|$
f23	t_{a1}	f48	v_2/v_1
f24	t_{b1}	f49	BMI
f25	t_{e1}		

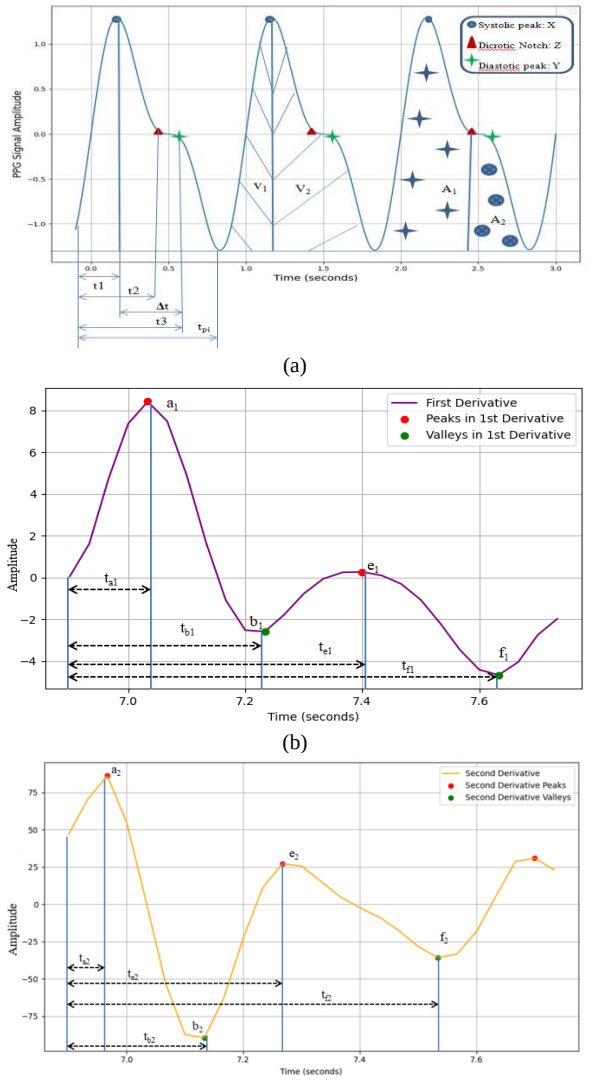

Fig. 10. Feature extraction from (a) Original "PPG wave", (b) "First derivative of PPG wave", and (c) "Second derivative of PPG wave".

VI. Feature Selection and Model Development

"GA" selected a subset of features from the "Red" and "Hue channels". GA is the feature optimization method inspired by natural evolution. It begins with an initial population of potential solutions (subsets of features), then iteratively selects the best candidates using crossover, mutation, and selection based on a fitness function (such as cross-validation performance). GA is highly effective in feature selection for complex problems where features interact with each other in non-obvious ways. It is especially suited for feature selection in medical datasets as it evolves mathematical expressions to find the optimal feature combination that minimizes prediction errors. The object function is represented mathematically as in Eq. (6).

$$Obj = Min(\mathcal{E}) + \lambda * \quad (6)$$

Where:

$\mathcal{E}$: Error represents the deviation of predicted values from the actual values.

λ: Regularization parameter controlling the trade-off between accuracy and simplicity.

C: Complexity refers to the overall intricacy of the chosen features.

The "DEAP (Distributed Evolutionary Algorithms in Python) library" is a powerful and flexible framework for implementing evolutionary algorithms such as GA. Feature selection started with all available features, and the process continued through elimination until the optimal outcomes were obtained.. This process aimed to identify the most significant features contributing to the prediction performance of regression models. In this study, different regression models, including "CatBoost", "XGBoost", "RFR", and "Gradient Boosting", were utilized to estimate blood glucose levels, with the features selected through a GA for optimal predictive performance. This study explored various control parameter settings of the GA to enhance accuracy while reducing the number of features. The optimal performance was achieved with "100 generations, a population size of 50, a crossover probability of 0.8, and a mutation probability of 0.1", which successfully identified the most important features for better predictive accuracy. When applied to "RGB" and "HSV color spaces", the number of selected features varies for different regression models.

VII. Result and Discussion

A total of 234 subjects were participated in the study, with fingertip video data recorded using a smartphone camera and an NIR LED module. For each subject, a 15-second video was captured, initially in the "RGB color space" and then converted to the "HSV color space" for further analysis. Several preprocessing techniques were employed to extract the "PPG wave" from both color spaces. Various "time-domain and frequency-domain" features were extracted from the original "PPG wave" as well as from its "derivatives". Additionally, demographic information such as "age, gender, and BMI" was incorporated as additional features. Several regression models were evaluated for predictive performance, and the XGBoost model demonstrated superior results in both the "RGB and HSV color spaces", highlighting its effectiveness and robustness in accurately estimating the target variable.

The effectiveness of the model was accessed using the R^2 score and MAE. R^2 and MAE were chosen as performance metrics due to their complementary natureR^2 indicates the fraction of variance accounted for by the model, reflecting its

goodness-of-fit, while MAE offers a straightforward measure of prediction accuracy by calculating the average error magnitude, making it resistant to outliers. The assessment metrics are mathematically defined by the Eq. (7) and (8). Furthermore, consistency analysis was performed using "Bland-Altman", "scatter plots", and "Clarke grid analysis". It is worth mentioning that all the results from these analyses were obtained from the 30% test dataset.

$$MAE = \frac{1}{n}\sum_{i=1}^{n}\left|y_{actual} - y_{predicted}\right| \quad (7)$$

$$R^2 = 1 - \frac{\sum_{i=1}^{n}(y_{actual} - y_{predicted})^2}{\sum_{i=1}^{n}(y_{actual} - y_{mean\_of\_actual})^2} \quad (8)$$

Where, y_{actual}: actual blood glucose value,

$y_{predicted}$: predicted blood glucose value,

$y_{mean\_of\_actual}$: mean of actual blood glucose values.

As shown in Table II, "XGBoost", "CatBoost", "RFR", and "Gradient Boosting Regression" algorithms were tested and compared to evaluate their predictive performance for estimating BGL. The GA for feature selection resulted in varying numbers of features being selected across these models, highlighting differences in how each algorithm assessed feature importance and interacted with the selected feature set. These variations can be attributed to model-specific characteristics, such as feature selection criteria, regularization techniques, and sensitivity to over fitting and redundancy. Among the models, "XGBoost" emerged as the top performer, providing the highest R-squared values in "RGB" and "HSV color spaces". "XGBoost" outperformed other models due to its strong regularization capabilities, which prevent over fitting in high-dimensional datasets, and its ability to effectively capture complex, nonlinear relationships and feature interactions. In the "RGB color space", "XGBoost" achieved an R^2 value of 0.89 and MAE of 19.89, indicating a strong correlation between predicted and actual BGL, which signifies high predictive accuracy. In the "HSV color space", "XGBoost" delivered an R^2 value of 0.84 and MAE of 24.76, demonstrating solid performance, though slightly lower than in RGB.

TABLE II. RESULTS OF MACHINE LEARNING MODELS IN "RGB" AND "HSV COLOR SPACE"

Color space	Model	Number of features selected	R^2	MAE
RGB	XGBoost	19	0.89	19.29
	CatBoost	21	0.82	23.43
	RFR	19	0.79	25.08
	Gradient Boosting	23	0.78	30.94
HSV	XGBoost	27	0.84	24.76
	CatBoost	20	0.82	25.09
	Gradient Boosting	30	0.72	27.44
	RFR	23	0.65	34.46

To evaluate the accuracy of the best-performing "XGBoost model", regression plots, "Clarke grid analysis", and "Bland-Altman plots" were utilized in both color spaces. A regression plot visually illustrates the association between the predictor and response variables in regression analysis. It demonstrates how accurately the model's predictions match the actual data. Fig. 11(a) and (b) illustrates the regression plots for the best-performing "XGBoost model" across the "RGB" and "HSV color spaces". The regression plot revealed a significant association between the predicted and reference BGL values in the "RGB color space", with most data points closely aligned around the regression line, particularly when compared to the "HSV color space".

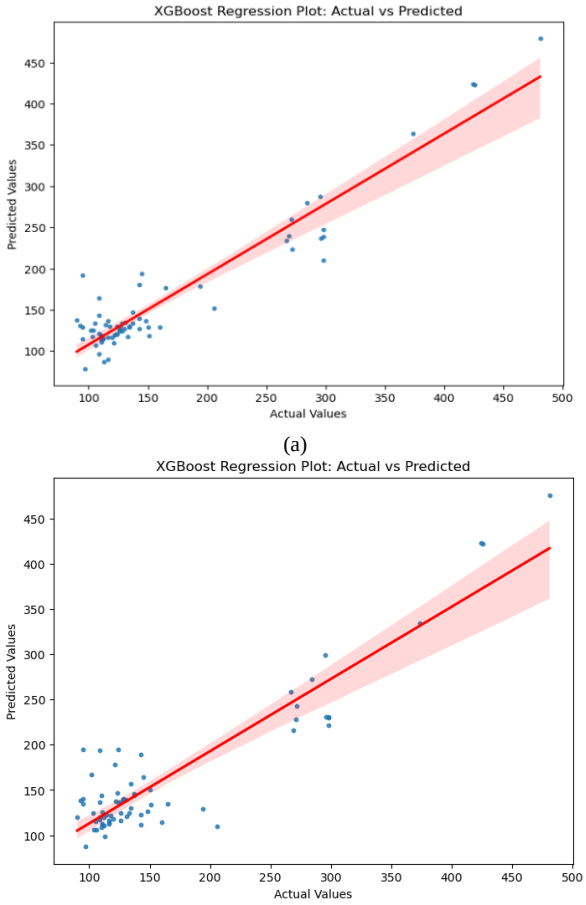

Fig. 11. Regression plot (a) "RGB color space", (b) "HSV color space".

The "Bland-Altman plot" is a visual technique for comparing two measurement techniques. It charts the discrepancies between the methods against their averages, with horizontal lines representing the average difference and the boundaries of agreement, calculated as the average difference ±1.96 times the standard deviation. It was found that only 7.04% of the BGL values fall outside the limits of agreement (±1.96 SD) for the testing dataset in "RGB" and "HSV color spaces", as illustrated in Fig. 12(a) and (b). This demonstrates a high level of agreement between the actual and estimated values.

"Clarke Error Grid Analysis" is widely recognized for validating BGL estimations. The grid is divided into five regions. "Region A" shows predictions within 20% of the actual BGL value. "Region B" includes predictions more than 20% off but not false. "Region C" highlights false positives indicating

incorrect “hypoglycemia” or “hyperglycemia”. “Region D” represents missed “hypoglycemia” or “hyperglycemia” cases, while “Region E” shows errors potentially misclassifying “hypoglycemia” or “hyperglycemia”.

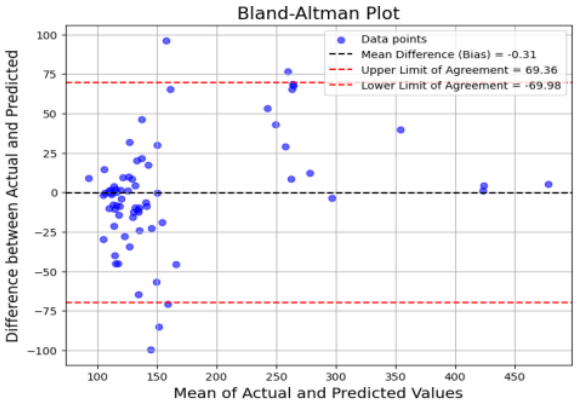

(a)

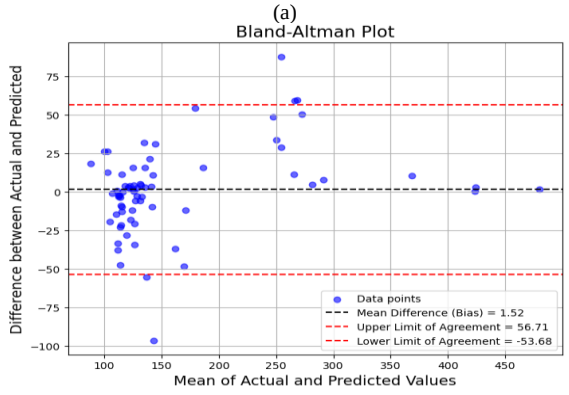

(b)

Fig. 12. Bland Altman plot (a) “RGB color space”, (b) “HSV color space”.

Fig. 13(a) illustrated the distribution of predictions for the “RGB color space”. “Region A” comprised 71.83% of the predictions within 20% of the actual BGL value, and “Region B” represented 19.72% of the predictions. “Region C”, on the other hand, included only 8.45% of the predictions. More than 90% of the data was concentrated in “Regions A and B”, deemed acceptable zones, indicating that most predictions were within a reasonable margin of error from the actual BGL values. Fig. 13(b) showed the prediction distribution for the “HSV color space”, with “Region A” represented 69.01% of predictions within 20% of the actual BGL value and “Region B” accounted for 15.49%. Region C contained 15.49% of false predictions. Around 85% of the predictions were found within “Regions A and B”, suggesting that most predictions were reasonably close to the actual BGL values, with only a tiny portion of the data fell into the false prediction range. In both color spaces, “Regions D and E” contained no data, which suggests that all predictions are confined to the acceptable or marginally acceptable ranges. The results showed that GA effectively selected relevant features for the “Red channel” in the “RGB color space” and the “Hue channel” in the “HSV color space”. While the “Red channel” provided a higher R^2 score, the “Hue channel” still performed well.

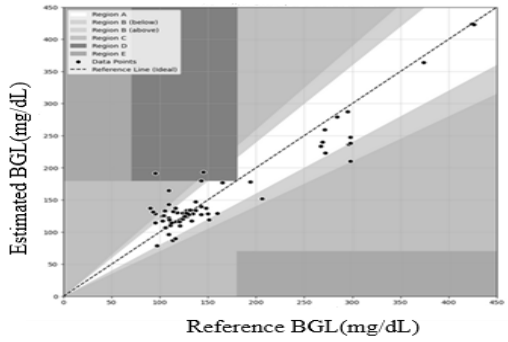

(a)

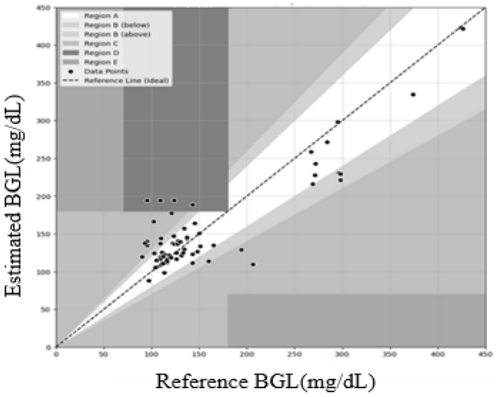

(b)

Fig. 13. Clarke Error Grid analysis for (a) “RGB color space”, (b) “HSV color space”.

Table III presented a comparative analysis between the proposed method and several existing contact and non-contact video-based blood glucose level (BGL) estimation approaches. Notably, all previous methods listed in the table performed BGL estimation exclusively within the RGB color space. In contrast, the proposed method explored additional spectral domains beyond RGB, offering a distinct approach to video-based BGL estimation.

By independently analyzing both color spaces, this study provided a detailed exploration of the unique contributions of the RGB and HSV color spaces in feature extraction and BGL estimation performance. The RGB color space achieved an R^2 value of 0.89, indicating good predictive accuracy under controlled settings, whereas the HSV color space yielded an R^2 value of 0.84, demonstrating strong performance despite being slightly lower. This difference suggested that while the “RGB color space” was effective in scenarios with stable lighting, the “HSV color space” offered better adaptability in more variable real-world conditions.

The dual analysis of “RGB” and “HSV color spaces” provided practical insights for the design of future non-invasive glucose monitoring systems. Depending on specific environmental conditions, device compatibility, and required robustness, researchers could make informed decisions on the most suitable color space to optimize estimation accuracy and reliability.

TABLE III. COMPARISON OF PROPOSED METHOD WITH SEVERAL EXISTING VIDEO BASED BLOOD GLUCOSE ESTIMATION METHODS

Reference	Device	Color Space	Number of Subjects	Algorithms	Results
Golap et al. [16]	Nexus- 6p	RGB	111	MGGP	R^2=0.88
Haque et al. [17]	Nexus- 6p	RGB	93	DNN	R^2=0.90
Islam et al. [22]	OnePlus 6T	RGB	52	PLS	standard error of prediction (SEP) =17.02 mg/dL
Nie et al. [25]	Medviv MV-NIR30-A industrial Near Infrared camera	RGB	8	RFR	R^2=0.60
Proposed work	Samsung A51	RGB HSV	234	XGBoost	R^2=0.89 R^2=0.84

VIII. CONCLUSION

A noninvasive BGL prediction model is proposed based on fingertip video data recorded using a smartphone in both "RGB" and "HSV color spaces". The GA is applied for feature selection in the "Red" and "Hue channels". "XGBoost" performed the best, achieving an R^2 value of 0.89 in the "RGB color space" and 0.84 in the "HSV color space". Bland-Altman analysis revealed that only 7.04% of BGL values fell outside the agreement limits for both color spaces. Even though the proposed method demonstrated superior performance on the collected data samples, its generalization is limited due to the relatively small dataset size. Additionally, the dataset did not include data from children under 18 or pregnant women, which restricts the applicability of the results to these specific populations. All data were collected using a single smartphone model (Samsung A51), which may impact the generalizability of the approach across different camera hardware. The experiments were conducted in controlled indoor environments, and as such, the model's performance in real-world conditions—where lighting and background variability are more pronounced—remains to be validated. Furthermore, the participant pool was limited, potentially affecting the model's robustness across diverse demographic groups. The study also focused solely on RGB and HSV color spaces, without exploring other potentially valuable color models.

In the future, efforts should focus on addressing these limitations by expanding the dataset to include more diverse populations and varying environmental conditions. Investigating and implementing innovative approaches to improve both the accuracy and efficiency of the system will also be a key direction. In particular, exploring alternative color spaces and their combinations may help capture more detailed and precise color information. Identifying optimal configurations could lead to better estimation results while reducing computational complexity. Additionally, incorporating advanced feature optimization techniques and a broader set of regression models could further enhance the accuracy and reliability of BGL estimation, ultimately contributing to the development of more robust and scalable non-invasive monitoring systems.

REFERENCES

[1] International Diabetes Federation, "Facts & Figures. IDF Diabetes Atlas 10th edition," IDF Diabetes Atlas, 10th ed., 2023. [Online]. Available: https://diabetesatlas.org/atlas/tenth-edition/. [Accessed: Dec. 20, 2024].

[2] A. Chopra, R. R. Rao, S. U. Kamath, S. A. Arun, and L. Shettigar, "Predicting blood glucose level using salivary glucose and other associated factors: A machine learning model selection and evaluation study," Informatics Med. Unlock, vol. 48, article 101523, 2024. [Online].

[3] D. Rodin, M. Kirby, N. Sedogin, Y. Shapiro, A. Pinhasov, and A. Kreinin, "Comparative accuracy of optical sensor-based wearable system for non-invasive measurement of blood glucose concentration," Clin. Biochem., vol. 65, pp. 15–20, Mar. 2019.

[4] Y. Tanaka, C. Purtill, T. Tajima, M. Seyama, and H. Koizumi, "Sensitivity improvement on CW dual-wavelength photoacoustic spectroscopy using acoustic resonant mode for noninvasive glucose monitor," in Proc. 2016 IEEE SENSORS, pp. 1–3, 2016.

[5] R. Kasahara, S. Kino, S. Soyama, and Y. Matsuura, "Noninvasive glucose monitoring using mid-infrared absorption spectroscopy based on a few wavenumbers," Biomed. Opt. Express, vol. 9, no. 1, pp. 289–302, Dec. 20, 2017.

[6] E. Monte-Moreno, "Non-invasive estimate of blood glucose and blood pressure from a photoplethysmograph using machine learning techniques," Artif. Intell. Med., vol. 53, no. 2, pp. 127–138, Oct. 2011.

[7] S. Habbu, M. Dale, and R. Ghongade, "Estimation of blood glucose by non-invasive method using photoplethysmography," Sādhanā, vol. 44, 2019.

[8] P. Jain, A. M. Joshi, and S. P. Mohanty, "iGLU: An intelligent device for accurate noninvasive blood glucose-level monitoring in smart healthcare," IEEE Consum. Electron. Mag., vol. 9, no. 1, pp. 35–42, Jan. 1, 2020.

[9] A. M. Joshi, P. Jain, S. P. Mohanty, and N. Agrawal, "iGLU 2.0: A new wearable for accurate non-invasive continuous serum glucose measurement in IoMT framework," IEEE Trans. Consum. Electron., vol. 66, no. 4, pp. 327–335, Nov. 2020.

[10] G. Hammour and D. P. Mandic, "An in-ear PPG-based blood glucose monitor: A proof-of-concept study," Sensors, vol. 23, article 3319, 2023.

[11] E. Mejía-Mejía, J. Allen, K. Budidha, C. El-Hajj, P. A. Kyriacou, and P. H. Charlton, "Photoplethysmography signal processing and synthesis," Photoplethysmography, vol. 4, pp. 69-146, 2022.

[12] Statista, "Forecast of smartphone users in India," Statista. [Online]. Available: https://www.statista.com/statistics/467163/forecast-of-smartphone-users-in-india/. [Accessed: Dec. 20, 2024].

[13] PwC, "mHealth expected to be crucial in making healthcare accessible in India: PwC-CII paper," PwC India. [Online]. Available: https://www.pwc.in/press-releases/2017/mhealth-expected-to-be-crucial-in-making-healthcare-accessible-in-india-pwc-cii-paper.html. [Accessed: Dec. 20, 2024].

[14] R. Zaman, C. H. Cho, K. Hartmann-Vaccarezza, T. N. Phan, G. Yoon, and J. W. Chong, "Novel fingertip image-based heart rate detection methods for a smartphone," Sensors (Basel), vol. 17, no. 2, article 358, Feb. 12, 2017.

[15] E. J. Wang, W. Li, D. Hawkins, T. Gernsheimer, C. Norby-Slycord, and S. N. Patel, "HemaApp: noninvasive blood screening of hemoglobin using smartphone cameras," in Proc. 2016 ACM Int. Joint Conf. Pervasive Ubiquitous Comput., 2016, pp. 593–604.

[16] Md. A. Golap, S. M. T. Uddin Raju, Md. R. Haque, and M. M. A. Hashem, "Hemoglobin and glucose level estimation from PPG characteristics features of fingertip video using MGGP-based model," Biomed. Signal Process. Control, vol. 67, article 102478, 2021.

[17] M. R. Haque, S. M. T. U. Raju, M. A. -U. Golap, and M. M. A. Hashem, "A novel technique for non-invasive measurement of human blood component levels from fingertip video using DNN-based models," IEEE Access, vol. 9, pp. 19025–19042, 2021.

[18] M. K. Hasan, M. Haque, N. Sakib, R. Love, and S. I. Ahamed, "Smartphone-based human hemoglobin level measurement analyzing pixel intensity of a fingertip video on different color spaces," Smart Health, vol. 5–6, pp. 26–39, 2018.

[19] M. K. Hasan, N. Sakib, J. Field, R. R. Love, and S. I. Ahamed, "A novel technique of noninvasivehemoglobin level measurement using HSV value of fingertip image," arXiv, 2019. [Online]. Available: https://arxiv.org/abs/1910.02579.

[20] Z. Fan, Y. Zhou, H. Zhai, Q. Wang, and H. He, "A smartphone-based biosensor for non-invasive monitoring of total hemoglobin concentration in humans with high accuracy," Biosensors, vol. 12, article 781, 2022.

[21] G. Zhang et al., "A noninvasive blood glucose monitoring system based on smartphone PPG signal processing and machine learning," IEEE Trans. Ind. Informat., vol. 16, no. 11, pp. 7209–7218, Nov. 2020.

[22] T. T. Islam, M. S. Ahmed, M. Hassanuzzaman, S. A. Bin Amir, and T. Rahman, "Blood glucose level regression for smartphone PPG signals using machine learning," Appl. Sci., vol. 11, article 618, 2021.

[23] M. M. Haque, F. Kawsar, M. Adibuzzaman, et al., "e-ESAS: Evolution of a participatory design-based solution for breast cancer (BC) patients in rural Bangladesh," Pers. Ubiquit. Comput., vol. 19, pp. 395–413, 2015.

[24] T.-T. Wei, H.-Y. Tsai, C.-C. Yang, W.-T. Hsiao, and K.-C. Huang, "Noninvasive glucose evaluation by human skin oxygen saturation level," 2016 IEEE International Instrumentation and Measurement Technology Conference Proceedings, Taipei, Taiwan, 2016, pp. 1-5.

[25] Z. Nie, M. Rong, and K. Li, "Blood glucose prediction based on imaging photoplethysmography in combination with machine learning," Biomed. Signal Process. Control, vol. 79, Part 2, article 104179, 2023.

[26] L. Chen, A. Reisner, and J. Reifman, "Automated Beat Onset and Peak Detection Algorithm for Field-Collected Photoplethysmograms," Conference Proceedings: Annual International Conference of the IEEE Engineering in Medicine and Biology Society, 2009, pp. 5689-5692.

[27] M. Z. Suboh, R. Jaafar, N. A. Nayan, N. H. Harun, and M. S. F. Mohamad, "Analysis on Four Derivative Waveforms of Photoplethysmogram (PPG) for Fiducial Point Detection," Front. Public Health, vol. 10, p. 920946, Jun. 2022.

[28] D. McDuff, S. Gontarek, and R. W. Picard, "Remote detection of photoplethysmographic systolic and diastolic peaks using a digital camera," IEEE Trans. Biomed. Eng., vol. 61, no. 12, pp. 2948-2954, Dec. 2014.

[29] K. Takazawa, N. Tanaka, M. Fujita, O. Matsuoka, T. Saiki, M. Aikawa, S. Tamura, and C. Ibukiyama, "Assessment of vasoactive agents and vascular aging by the second derivative of photoplethysmogram waveform," Hypertension, vol. 32, no. 2, pp. 365-370, Aug. 1998.

[30] U. Rubins, A. Grabovskis, J. Grube, and I. Kukulis, "Photoplethysmography analysis of artery properties in patients with cardiovascular diseases," in 14th Nordic-Baltic Conference on Biomedical Engineering and Medical Physics, A. Katashev, Y. Dekhtyar, and J. Spigulis, Eds., IFMBE Proceedings, vol. 20, Springer, Berlin, Heidelberg, 2008, pp. 319–322.

[31] S. A. Esper and M. R. Pinsky, "Arterial waveform analysis," Best Pract. Res. Clin. Anaesthesiol., vol. 28, no. 4, pp. 363-380, Dec. 2014.

[32] E. R. Seitsonen, I. K. Korhonen, M. J. van Gils, M. Huiku, J. M. Lötjönen, K. T. Korttila, and A. M. Yli-Hankala, "EEG spectral entropy, heart rate, photoplethysmography and motor responses to skin incision during sevoflurane anaesthesia," Acta Anaesthesiol. Scand., vol. 49, no. 3, pp. 284-292, Mar. 2005.

[33] J. B. Hyun, S. K. Jung, S. K. Yun, B. Lee, and S. K. Park, "Second derivative of photoplethysmography for estimating vascular aging," Proceedings of the IEEE/EMBS Region 8 International Conference on Information Technology Applications in Biomedicine (ITAB), 2007, pp. 70-72.

[34] Z. Xiao, Y. Lyu, X. Hu, Z. Hu, Y. Shi, and H. Yin, "Evaluating photoplethysmogram as a real-time cognitive load assessment during game playing," Int. J. Hum.-Comput. Interact., vol. 34, pp. 1-12, Apr. 18, 2018.

[35] J. R. Koza, “Genetic programming as a means for programming computers by natural selection,” Statistics and Computing, vol. 4, no. 2, pp. 87–112, Jun. 1994.

[36] P. Thanathamathee, S. Sawangarreerak, S. Chantamunee, and D. N. Mohd Nizam, “SHAP-Instance Weighted and Anchor Explainable AI: Enhancing XGBoost for Financial Fraud Detection,” Emerging Science Journal, vol. 8, no. 6, pp. 2404–2430, Dec. 2024, doi: 10.28991/esj-2024-08-06-016.